Feasibility study on ultra-low dose 3D scout of organ based CT scan planning

Zhye Yin[1*], Yangyang Yao[2], Albert Montillo[3], Peter M Edic[4], Bruno De Man[1]
[1]CT Systems and Application Laboratory, GE Global Research, Niskayuna, NY
[2]X-ray and CT Laboratory, GE Global Research, Shanghai, China
[3]Biomedical Image Analysis Laboratory, GE Global Research, Niskayuna, NY
[4]CT, X-ray and Functional Imaging, GE Global Research, Niskayuna, NY
[*]yin@research.ge.com

***Abstract*—3D volumetric CT images hold the potential to become a rich source of information for 3D organ segmentation and far exceed that made available through 2D radiograph images. Acquiring and generating 3D volumetric images for scan preparation purposes, i.e. 3D scout, while delivering radiation dose equivalent to conventional 2D radiograph is challenging. We explore various acquisition parameters and post-processing methods to reduce dose of a 3D scout while reducing the noise and maintaining the edge strength around the target organ. We demonstrated that similar edge strength and noise to the conventional dose CT scan can be achieved with 3D scout acquisition and post-processing while being dose neutral to a 2D scout acquisition.**

Keywords— CT acquisition protocol; low dose; 3D scout; organ segmentation; IQ metric

I. INTRODUCTION

Segmentation or extraction of organ boundaries from the 2D radiograph preparatory scans, i.e. 2D scouts, has been explored before [1-3]. Due to overlapping nature of tissues projected onto a 2D scout, segmentation of adjacent soft tissue organs has proven to be very challenging. In a clinical setting, 3D helical acquisitions are often used to precisely localize target organs before the main scan but the radiation dose for such preparatory scans is quite high. In this paper, we propose a 3D volumetric preparatory scan, i.e. 3D scout, to segment target organs for scan planning while delivering radiation dose similar to conventional 2D scout.

The dose from a conventional 2D scout acquisition is a small fraction of the dose from the main scan, typically 0.4%-2%. Therefore, acquiring an ultra-low dose 3D scout delivering similar dose to conventional 2D scout while maintain image quality sufficient for organ segmentation is immensely challenging. Reconstructed images from such a low dose acquisition contain high noise and image artifacts such as streaks. Consequently conventional edge and region based image segmentation methods [4-5] tend to yield low segmentation accuracy [6-8]. More advanced model based organ segmentation (MBS) methods hold greater potential to overcome some of these challenges, however even these can fail when the noise or streaks are prominent [9-11].

In this work, we explored various ultra-low dose acquisition and post-processing strategies to reduce the radiation dose of a 3D scout. To evaluate each strategy, we defined the image quality metrics that reflect organ 'segmentability', i.e. ability to segment, rather than using a specific segmentation approach so that our experiments are largely independent of the specific organ segmentation algorithm. Though multiple body regions such as head, chest and abdomen are routinely scanned, we focus on the abdomen and specifically the liver organ since it is one of the most challenging organs due to its shape complexity, intersubject shape variability, and low boundary contrast. However it is straightforward to extend our work and methodology to other organs and applications.

Table I. Key DOE parameters

DOE	mA	rotation speed	mAs	# of views	dose%	
Without noise reduction techniques						
1	2000	0.4	800	1000	N/A	Ground Truth
2	600	0.4	240	1000	100%	Baseline
3	240	0.4	24	250	10%	Pulsed Acq.
4	240	0.4	12	125	5%	Pulsed Acq.
5	120	0.4	12	250	5%	Pulsed Acq.
6	120	0.4	6	125	2.5%	Pulsed Acq.
7	60	0.4	6	250	2.5%	Pulsed Acq.
8	60	0.4	3	125	1.25%	Pulsed Acq.
Noise Reduction techniques						
9	60	0.4	3	125	1.25%	Detector rebin(4)
10	60	0.4	3	125	1.25%	Detector rebin(9)
11	60	0.4	3	125	1.25%	Smooth Kernel
12	60	0.4	3	125	1.25%	Fast Iter. Recon
Combination of noise reduction techniques						
13	60	0.4	3	125	1.25%	Kernel+D.Rebin
14	60	0.4	3	125	1.25%	Kernel+Rebin+Iter
Electronic Noise Reduction						
15	60	0.4	12	250	5%	2x exposure
16	60	0.4	6	125	2.5%	2x exposure
17	60	0.4	3	62	1.25%	2x exposure

II. METHODOLOGY

To achieve ultra-low dose for 3D scout, we proposed two low dose acquisition methods and three post-processing and reconstruction approaches.

For low dose acquisition, we reduced the dose of 3D scout by reducing mA and by reducing the number of views while maintain same exposure time per view, i.e. by

emulating pulsed acquisition. Detailed acquisition parameters in our design of experiments (DOE) are shown in Table 1, DOE1-DOE8. To simulate ultra-low dose 3D scout, we use CATSIM with the anthropomorphic xCAT phantom [12-13]. A 3rd generation axial scan mode is adopted for simplicity and 8 rows of detectors are positioned over the liver region.

We simulated three denoising and reconstruction techniques: detector rebinning, smooth reconstruction kernel and fast iterative reconstruction algorithm such as ASIR, shown in Table 1, DOE9-14. Since organ segmentation algorithms mostly utilize the gradient information along the boundary, spatial resolution becomes less critical for the success. First, we proposed 2 by 2 and 3 by 3 detector rebinning approaches where the detector cells in neighboring rows and columns, 4 pixels and 9 pixels respectively, are combined into one effective cell. Second, since filter kernels for the FBP type reconstruction algorithms can be tuned to yield smooth and less noisy images, we select the smoothest reconstruction kernel available which can be aggressively modified further to achieve more smoothing in future. Finally, we emulated fast iterative reconstruction which typically has 50% noise reduction capability by simulating multiple acquisitions at same location with random noise seeds and averaging those runs.

Since electronic noise in CT acquisition sometimes dominates overall noise characteristic and makes it difficult to de-noise, we additionally simulated acquisitions with prolong exposure and compared the difference, shown in Table 1, DOE15-17.

All images are reconstructed with conventional FBP reconstruction algorithm with 1mm by 1mm by 0.625mm voxel size. The DFOV is 360mm and scan time per revolution is 0.4s. We simulated a noiseless scan, shown in Table 1, DOE1 and a conventional main scan with 240mA·s, shown in Table 1, DOE2. The dose percentage shown in the last column in Table 1 was computed relative to DOE2, the conventional main scan.

We devised two image quality metrics for organ segmentability. The first metric measures the noise at the interior portion of liver using 2cm by 2cm rectangular region of interest (ROI), shown as dotted box in Figure 1(a). The organ interior noise σ is expressed as the standard deviation of voxel intensities from a ROI in the liver interior:

$$\sigma = stdev(rectangular\ ROI), \quad (1)$$

The success of organ segmentation in ultra-low dose 3D scout is highly dependent of the contrast changes along the boundary of organ. High frequency artifacts such as streaks, increased noise, and blurred boundary due to heavy post-processing all can impair the success of organ segmentation. To measure the strength of the contrast change at the boundary, we propose a new metric, normalized edge strength (NES) which adds normalization to prior metrics [14]. We manually extract the ground truth boundary from the liver in the reconstruction image of xCAT phantom using VV 4D slicer [15]. This boundary is represented by a piecewise linear polygonal curve and shown in blue in Figure 1(b). We extract the intensity profile along this curve from the image and denote the intensity profile along the boundary curve as *c(t)* were *t* parameterizes arc length along *c*, i.e. boundary curve. A clearly defined edge will have a high intensity gradient perpendicular to the boundary and a low gradient parallel to the boundary. To measure the perpendicular gradient, we evenly distribute 7mm line segments straddling the boundary, illustrated with green line segments in Figure 1(b). We extract the intensity profiles along those line segments and denote them as *s(r)* where *r* parameterizes arc length along *s*, i.e. line segment. Finally, we define the normalized edge strength (NES) of a boundary as:

$$NES = \frac{trimmean\left(\left\{max\left|\frac{ds_i(r)}{dr}\right|\right\}_{i=1}^{N}, 5\right)}{trimmean\left(\left\{\left|\frac{dc(t)}{dt}\right|\right\}, 5\right)} \quad (2)$$

For robustness to outliers, instead of taking average of gradients, we trimmed the highest and the lowest 2.5% values. For a vector input v, the trimmean(v,5) function computes the mean of elements in v, excluding the highest and lowest 2.5% values.

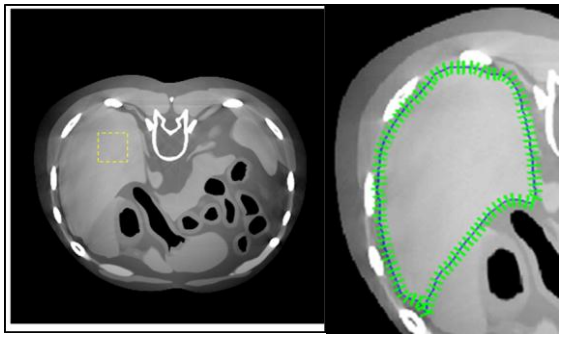

Figure 1: (a) liver region with 2cm by 2cm rectangular ROI in yellow for noise measurement (b) interpolated ground truth contour to measure NES (magnified view)

III. Results and Analysis

The reconstructed images at iso-plane for each DOE are shown in Figure 2. Qualitatively we observe that as mA and number of views drop, images rapidly lose soft tissue contrast and the boundary of liver becomes invisible, shown in Figure 2(6), (7) and (8). Images with combination of various denoising techniques result in noisy but more visible organ boundaries, shown in Figure 2(10), (13) and (14). Especially, the image processed with the combination of 9-pixel detector rebinning, smooth reconstruction kernel and fast iterative reconstruction, shown in Figure 2(14), presents with well-defined liver boundary while delivering only fraction of dose, 1.25%, from the baseline (DOE2, Figure 2(2)). By allowing twice the x-ray exposure time per view, electronic noise was suppressed, as shown in Figure 2(15), (16) and (17). To deliver similar dose while allowing longer exposure, the number of views was aggressively reduced to 62, only 6.2% of 1000 views in the baseline case. However, we observe that images reconstructed without dedicated sparse view reconstruction algorithm have very high noise and invisible organ boundaries, shown in Figure 2(17).

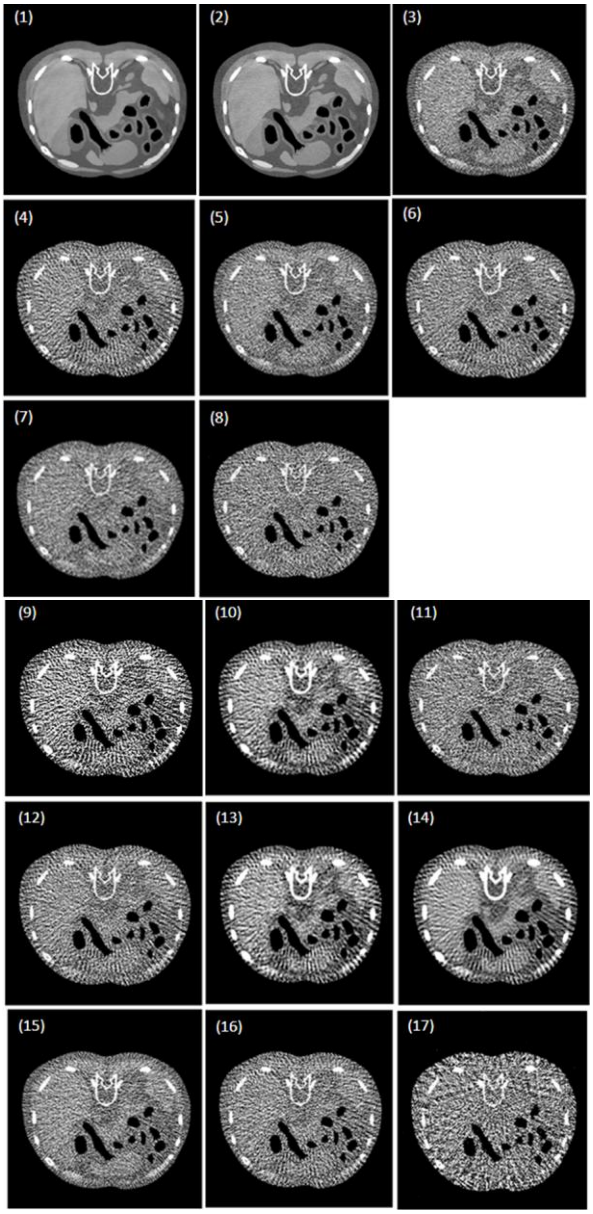

Figure 2: 3D scout with various acquisitions and post-processing techniques are shown. See Table 1 for details.

To objectively and quantitatively compare the performance of various simulated 3D scout acquisitions, we plot both image quality metrics and % dose for every DOE shown in Table 1. Noise performances of various 3D scout acquisitions and post processing techniques are shown by the blue line in Figure 3 while the red line shows corresponding % dose level. DOE1 was simulated with 2000mA to produce noise-free ground truth. DOE2 was simulated with 240mAs with full number of views and served as baseline. With combination of three de-noising approaches, the interior noise metric successfully reached the level of the baseline, DOE2, with only 1.25% of dose level in DOE2. Similarly, the performance of normalized edge strength (NES) of various 3D scout acquisitions and post processing techniques are shown by the blue line in Figure 4 while the red line indicates corresponding % dose level. We observe that normalized edge strength (NES) increases greatly for 2 by 2 and 3 by 3 detector rebinning technique, DOE9 and DOE10, while the dose percentage is as low as 1.25%. On the other hand, smooth reconstruction kernel and fast iterative reconstruction emulation don't improve normalized edge strength (NES) as much as detector rebinning. The combination of detector rebinning, smooth reconstruction kernel and fast iterative reconstruction techniques (DOE14) improves the normalized edge strength (NES) ever further, reaching nearly the level of full dose acquisition (DOE2).

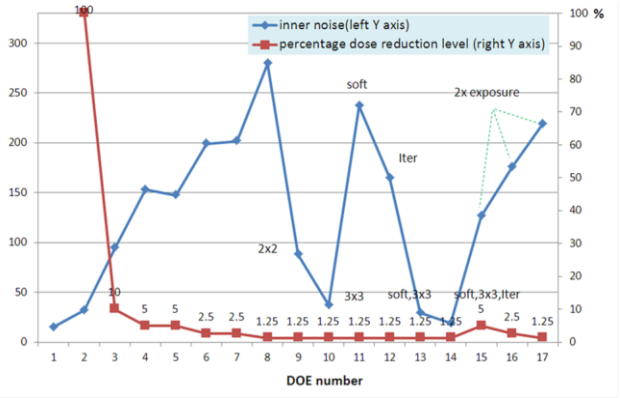

Figure 3: interior noise metric and % dose from 240mAs baseline scan are shown in red and blue lines respectively. Each detector rebinning is labeled as 2x2 and 3x3. Smooth reconstruction kernel is labeled "soft". Fast iterative reconstruction is labeled "Iter".

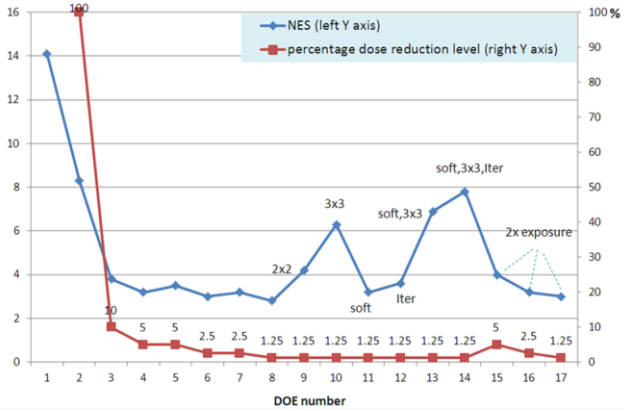

Figure 4: Normalized edge strength (NES) and % dose from 240mAs baseline scan are shown in red and blue respectively. Each detector rebinning is labeled as 2x2 and 3x3. Smooth reconstruction kernel is labeled as soft. Fast iterative reconstruction is labeled as Iter.

IV. Conclusion

We investigated the feasibility of 3D volumetric preparatory scan, i.e. 3D scout, with ultra-low dose that is comparable to the dose of a conventional 2D scout while providing sufficient image quality, especially edge strength and uniformity, to make soft tissue organ boundaries prominent to facilitate segmentation and subsequent scan planning purposes. We proposed to reduce dose by reducing

mA and the number of views while maintaining x-ray exposure time per view. We also proposed additional reconstruction and post-processing approaches to further improve image quality. We defined two image quality metrics to measure the edge strength at the boundary and noise uniformity inside of organs. We demonstrated that 3D scout can achieve equivalent image quality as a regular 240mAs diagnostic scan while delivering only 1.25% of dose. This work presents an approach that allows investigating the feasibility of 3D scout independent of the organ segmentation algorithm. In future, we plan to investigate the feasibility of 3D scout with further reduced streaking artifacts, to improve image quality visually and to further evaluate with learning-based organ localization algorithm that we are developing [2-3].

REFERENCES

[1] Tao, Y., Peng, Z., Krishnan, A., Zhou, X.: Robust learning-based parsing and annotation of medical radiographs. IEEE Transactions on Medical Imaging 30(2), 338-350 (2011)

[2] Montillo, A.*, Song, Q.*, Liu, X., Miller, J.: Parsing radiographs by integrating landmark set detection and multi-object active appearance models. In: SPIE Medical Imaging (2013)

[3] Qi Song*, Albert Montillo*, Roshni Bhagalia, and Srikrishnan V, Organ localization using joint AP/LAT view landmark consensus detection and hierarchical active appearance models, In Proc. of Medical Computer Vision Workshop, Medical Image Computing and Computer-Assisted Intervention (MICCAI), 2013

[4] Linda G. Shapiro and George C. Stockman (2001): "Computer Vision", pp 279-325, New Jersey, Prentice-Hall, ISBN 0-13-030796-

[5] R. C. Gonzalez and R.E. Woods, Digital Image Processing 2nd Edition, Prentice Hall, New Jersey, 2002

[6] Seifert, S., Barbu, A., Zhou, S., Liu, D., Feulner, J., Huber, M., Suehling, M., Cavallaro, A., Comaniciu, D.: Hierarchical parsing and semantic navigation of full body CT data. SPIE Medical Imaging 7259, 02:1-8 (2009)

[7] Potesil, V., Kadir, T., Platsch, G., Brady, M.: Personalization of pictorial structures for anatomical landmark localization. In: IPMI. pp. 333-345. Springer (2011)

[8] Zhang, S., Zhan, Y., Dewan, M., Huang, J., Metaxas, D., Zhou, X.: Deformable segmentation via sparse shape representation. Medical Image Computing and Computer-Assisted Intervention–MICCAI 2011 (2011) 451–458

[9] T.F. Cootes and C.J. Taylor and D.H. Cooper and J. Graham (1995). "Active shape models - their training and application". Computer Vision and Image Understanding (61): 38–59. [1]

[10] S. C. Mitchell, J. G. Bosch, B. P. F. Lelieveldt, R. J. van der Geest, J. H. C. Reiber, and M. Sonka. 3-d active appearance models: Segmentation of cardiac MR and ultrasound images. IEEE Trans. Med. Imaging, 21(9):1167–1178, 2002

[11] T.F. Cootes, G. J. Edwards, and C. J. Taylor. Active appearance models. ECCV, 2:484–498, 1998

[12] Bruno De Man, Samit Basu, Naveen Chandra, Bruce Dunham, Peter Edic, et al. "CatSim: a new computer assisted tomography simulation environment", Proc. SPIE 6510, Medical Imaging 2007: Physics of Medical Imaging, 65102G (March 14, 2007)

[13] W.P. Segars, M. Mahesh, T.J. Beck, E.C. Frey, B.M. Tsui, "Realistic CT simulation using the 4D XCAT phantom," Medical physics 35, 3800-3808 (2008).

[14] Montillo, J. Udupa, L. Axel, D. Metaxas, Interaction between noise suppression and inhomogeneity correction in MRI , In Proc. of SPIE: Medical Imaging, volume 5032, pages 1025-1036, 2003

[15] VV-4D slicer, an opensource image tool available from http://www.creatis.insa-lyon.fr/rio/vv/